Heliyon 7 (2021) e05902

Contents lists available at ScienceDirect

Heliyon

journal homepage: www.cell.com/heliyon

Research article

Time course of collateral vessel formation after retinal vein occlusion visualized by OCTA and elucidation of factors in their formation

Hajime Takahashi *, Kazuki Nakagawa, Haruhiko Yamada, Hidetsugu Mori, Shimpei Oba, Keiko Toyama, Kanji Takahashi

Department of Ophthalmology, Kansai Medical University, Hirakata, Osaka, Japan

ARTICLE INFO

Keywords:
OCTA
RVO
Collateral vessels

ABSTRACT

Background: It is clinically recognized that collateral vessels can form after retinal vein occlusion (RVO) in some cases and these vessels can lead to spontaneous recovery of the pathological condition. In recent years, optical coherence tomography angiography (OCTA) has become a decisive clinical instrument. Unlike previous angiography tests, OCTA enables the non-invasive visualization of fundus vasculature without the need for administration of a contrast agent. However, it remains to be determined if OCTA depicts the 'true' histological status as several studies have reported artifacts in OCTA imaging.

Methods: We generated a laser-induced mouse RVO model, and evaluated the subsequent formation of collateral vessels in order to understand the mechanisms by which collateral vessels form using OCTA imaging, as well as molecular and histological assessments.

Results: We succeeded in visualizing the time course of collateral vessel formation in a mouse RVO model and confirmed the similarity in formation of collateral vessels only within the deep layer of the retina in both human and mouse. We hypothesized that sphingosine 1-phosphate receptor-1 (S1PR1) may play important roles via vascular shear stress linking vein occlusion and collateral vessel formation. Results from OCTA revealed that collateral vessels are increased in response to administration of a S1PR1 agonist in a mouse RVO model. Based on quantitative reverse transcription polymerase chain reaction (qRT-PCR), S1PR1 messenger ribonucleic acid (mRNA) levels in the whole retina peaked 6 h after photocoagulation in this model. Immunohistochemical staining of retinal flat mounts revealed that S1PR1 staining occurred along the laser-occluded blood vessels.

Conclusion: We observed the temporal process of collateral vessel formation in a mouse RVO model and identified the relationship between S1PR1 and shear stress as one of the factors in collateral vessel formation in RVO.

1. Background/Introduction

Human retinal blood vessels often experience arteriosclerosis after middle age, which can lead to retinal vein occlusion and blood flow disorders. Disordered blood flow in the retina may cause retinal edema and impaired vision [1]. In some cases of retinal vein occlusion, collateral vessels can appear in the chronic stage [2]. Clinically, it is occasionally observed that the pathological conditions caused by retinal ischemia can recover spontaneously. Collateral vessels play a large role in this recovery [1]. To investigate the mechanisms of this natural healing process, fluorescein angiography has been widely used to evaluate leakage and blood vessel occlusion. However, there have been very few examples detailing how collateral vessels change over time [3, 4, 5]. This is because previously used angiography methods were extremely invasive in experimental animals such as mice, so this type of angiography could not be performed repeatedly over time. Optical coherence tomography angiography (OCTA) is a recently introduced technique for clinical use [6, 7]. OCTA is different from traditional angiography methods because it does not require any special contrast agent (i.e., fluorescein sodium for fluorescein angiography or indocyanine green (ICG) for ICG angiography). OCTA is thus less invasive to the body than traditional angiographies especially for those with drug allergies. Although experience and information on OCTA in human clinical use has been gradually increasing [1, 8, 9, 10, 11, 12, 13], there have been very few examples of applying this technique to experimental animal models [14]. Through the use of OCTA, retinal blood vessels in a mouse RVO model can be imaged multiple times with less invasion. Therefore, OCTA might be highly useful for evaluating vascular changes in animals over time [14].

* Corresponding author.
E-mail address: takahaj@hirakata.kmu.ac.jp (H. Takahashi).

https://doi.org/10.1016/j.heliyon.2021.e05902
Received 28 August 2020; Received in revised form 1 December 2020; Accepted 31 December 2020

Moreover, OCTA can separately visualize blood flow structures in the retinal blood vessels from multiple layers of the retina. The aim of the present study was to observe and investigate the changes in blood flow due to single retinal vein occlusion over time, and to investigate the mechanisms responsible for these changes. For this purpose, we developed a mouse RVO model in which we could visualize retinal blood vessels using OCTA. We hypothesized that shear stress due to abnormal blood flow may contribute to collateral vessel formation. It has been reported that shear stress within blood vessels themselves acts as an agonist of sphingosine 1-phosphate receptor-1 (S1PR1) on vascular endothelial cells, which causes vasodilation [15]. We speculated that a similar mechanism might function in a mouse RVO model, and thus we conducted the following experiments to test this hypothesis.

2. Materials and methods

2.1. Animals

All animal experiments followed the guidelines of the Association for Research in Vision and Ophthalmology (ARVO) Statement for the Use of Animals in Ophthalmic and Vision Research and were approved by Kansai Medical University (approval number: 17-106). Wild-type (WT) BALB/cA mice were purchased from CLEA Japan (Tokyo, Japan). A total of 73 female mice aged 6–8 weeks were used for this study. All mice were kept in pathogen-free plastic cages with 12-hour light-dark cycles and had continuous free access to water and food. All plastic cages, water, bedding and feed were purified before use. For all procedures, anesthetization was achieved by intraperitoneal injection of 90 mg/kg ketamine hydrochloride (Daiichi Sankyo Co., Tokyo, Japan) and 40 mg/kg xylazine (Bayer, Berlin, Germany), and pupils were dilated with topical 0.5% tropicamide and 0.5% phenylephrine (Santen Pharmaceutical, Osaka, Japan).

2.2. Preparation of retinal vein occlusion

Under deep anesthesia, BALB/cA female mice were intraperitoneally injected with 0.15 ml Phosphate-buffer saline (PBS) containing 5 mg/ml Rose Bengal dye (Nacalai-Tesque, Kyoto, Japan). Immediately after dye injection (during the period that the dye reaches the retinal blood vessels and until it disappears, approximately 3 min), the left eye of each mouse was subjected to photocoagulation (PC) using a GYC-2000 half wavelength YAG laser of 532 nm wavelength (NIDEK Co, Tokyo, Japan) attached to a slit-lamp delivery system (Carl Zeiss SL 130, Jena, Germany). A laser spot size of 100 μm, with a 100 ms pulse duration and a 200 mW incident power were applied to the target vessel to stop blood flow in the retinal vein. For the laser-induced occlusion, a single vessel which was 1–2 optic nerve diameters away from the optic nerve head was selected and coagulated.

2.3. Evaluation of collateral vessels

OCTA (RS-3000 Advance, the optical resolution is 20μm in the XY direction and 7μm in the Z direction, NIDEK Co, Tokyo, Japan) was used to evaluate retinal vascular changes and observe blood flow prior to and at days 3, 5, 7, and 14 after PC. We captured the image of occluded area including central retina by tilting the mouse head. After that, we created images by superimposing them by JTrim software (free software, Copyright: WoodyBells). Collateral vessels were defined as capillaries that became markedly dilated and tortuous compared to those prior to occlusion, regardless of the direction of progression. Retinal vasculature was histologically evaluated in fluorescein dye-perfused retinal flat mounts. To prepare a retinal flat mount specimen, deeply anesthetized mice were injected with 0.5 ml of 0.02 mg/ml albumin-fluorescein isothiocyanate conjugate (FITC; Sigma-Aldrich, St. Louis, MO, USA) dissolved in PBS into the tail vein. After administration, the mice were kept alive for one hour to allow the dye to sufficiently spread into the retinal blood vessels. Mice were then sacrificed by cervical dislocation, then the eyes were enucleated and fixed in 4% paraformaldehyde (FUJIFILM Wako Pure Chemical Co, Osaka, Japan) for 10 min. The retinas were then isolated from the eye, flattened and mounted with ProLong Gold antifade reagent (Life Technologies, Eugene, OR, USA). The processed retinal tissues were cover-slipped, then observed under a fluorescence microscope (BX50 with DP80 CCD camera, Olympus Co, Tokyo, Japan).

2.4. S1PR1 agonist and inverse agonist administration

A synthetic sphingosine-1-phosphate receptor 1 (S1PR1) agonist, SEW2871 (Cayman Chemical, Ann Arbor, MI, USA) and inverse-agonist, VPC23019 (Cayman Chemical, Ann Arbor, MI, USA), were dissolved in Dimethyl sulfoxide (DMSO, FUJIFILM Wako Pure Chemical Co, Osaka, Japan) to a concentration of 2 mg/ml (SEW) and 0.25 mg/ml (VPC) and administered intraperitoneally at a volume of 0.1 ml every day for three days beginning on the day of PC. We then observed the structural changes in the retinal vessels and compared them among 15 eyes from the non-administration (normal RVO) group, 9 eyes of the SEW-administration (RVO + SEW) group, and 7 eyes of the VPC-administration (RVO + VPC) group using OCTA. We also evaluated the appearance of retinal blood vessels from 2 eyes of a non-laser irradiated and non-administered (sham) group, 4 eyes of a non-laser irradiated and SEW-administration (sham + SEW) group, and 4 eyes of a non-laser irradiated and VPC-administration (sham + VPC) group, and compared these as controls.

2.5. qRT-PCR

All mice were euthanized by cervical dislocation after deep anesthesia as described above. Immediately after isolating the whole retinas from each eye, they were stored in RNA later® (Thermo Fisher Scientific, Waltham, MA, USA) to prevent degradation. The isolated retinas were then homogenized using a Biomasher (Nippi Inc., Tokyo, Japan). Total RNA was isolated using RNeasy Plus Mini® Kit (Qiagen, Venlo, The Netherlands) according to the manufacturer's protocol. Total RNA was reverse-transcribed to generate cDNA using the SuperScript® VILO™ cDNA Synthesis Kit (Thermo Fisher Scientific, Waltham, MA, USA). The reverse-transcribed cDNA was then subjected to qRT-PCR (Thermal Cycler Dice® Real Time System II; TAKARA Bio, Otsu, Shiga, Japan). qRT-PCR reactions were performed in a total volume of 25 μl using SYBR® Premix Ex TaqII™ PCR Kit (TAKARA Bio, Otsu, Shiga, Japan) following the manufacturer's protocol.

The target sequences used in this study were amplified with the following primers [16, 17].

Gapdh:
Forward, 5′-GACTTCAACAGCAACTCCCAC -3′
Reverse, 5′-TCCACCACCCTGTTGCTGTA -3′
S1PR1:
Forward, 5′-ACTACACAACGGGAGCAACAG -3′
Reverse, 5′-GATGGAAAGCAGGAGCAGAG -3′

Quantitative mRNA expression levels in each group were normalized to Gapdh mRNA levels as an internal control. mRNA expression levels in each group were calculated using relative quantification (standard curve method). For controls, we used mRNA from the entire retina of mice without PC and drug administration at 7 weeks after birth.

2.6. Immunohistochemical staining of retinal flat mounts

Deeply anesthetized mice were sacrificed by intracardial perfusion with PBS after thoracotomy. After PBS perfusion, eyes were enucleated and fixed in 4% paraformaldehyde for 10 min. Then, the anterior portion of the eyeball was dissected. The posterior portion of the eyeball was fixed again in 4% paraformaldehyde for 50 min. Whole retinas were then

isolated and permeabilized in PBS containing 4% Block Ace blocking reagent (DS Pharma Biomedical, Osaka, Japan) and 0.5% Triton X-100 for 3h at room temperature. The following antibodies were used for wholemount immunolabeling of the retina: anti-CD31 monoclonal antibody (rat anti-mouse CD31, 1:500; BD Biosciences Pharmingen, San Diego, CA, USA) was used to detect blood vessels with Alexa Fluor-568 secondary antibody (1:400); anti-S1PR1 monoclonal antibody (rabbit anti-mouse, rat S1PR1, 1:200; Almone Labs, Jerusalem, MA, USA) was used to detect S1PR1 with Alexa Fluor-488 secondary antibody (1:400). The isolated retinas were incubated in primary antibody solution at room temperature for 24 h with shaking. After several washes in PBS, retinas were incubated for 4 h at room temperature in secondary antibody solution. To flat mount, 4 cuts were made from the edge of the retina toward the center after thoroughly washing several times; retinas were then flattened and mounted with ProLong Gold antifade reagent and cover-slipped. Tissues were observed with a fluorescence microscope (BX50 with DP80 CCD camera, Olympus Co, Tokyo, Japan).

2.7. Statistical analysis

The number of collateral vessels per eye was measured by two masked independent graders, and data were analyzed by correlation coefficients and Bland-Altman plots. The average number of collateral vessels was analyzed by ANOVA and post-hoc tests (Tukey-Kramer method).

S1PR1/Gapdh mRNA expression levels in whole retinas quantified by RT-PCR were analyzed by ANOVA and post-hoc tests (Tukey-Kramer method). All tests were performed and analyzed using JMP software (SAS Institute Inc., Caly, NC, USA). P values <0.05 were considered statistically significant. We confirmed that all data were normally distributed using a normal distribution point plot and Shapiro-Wilk test and O'Brien test.

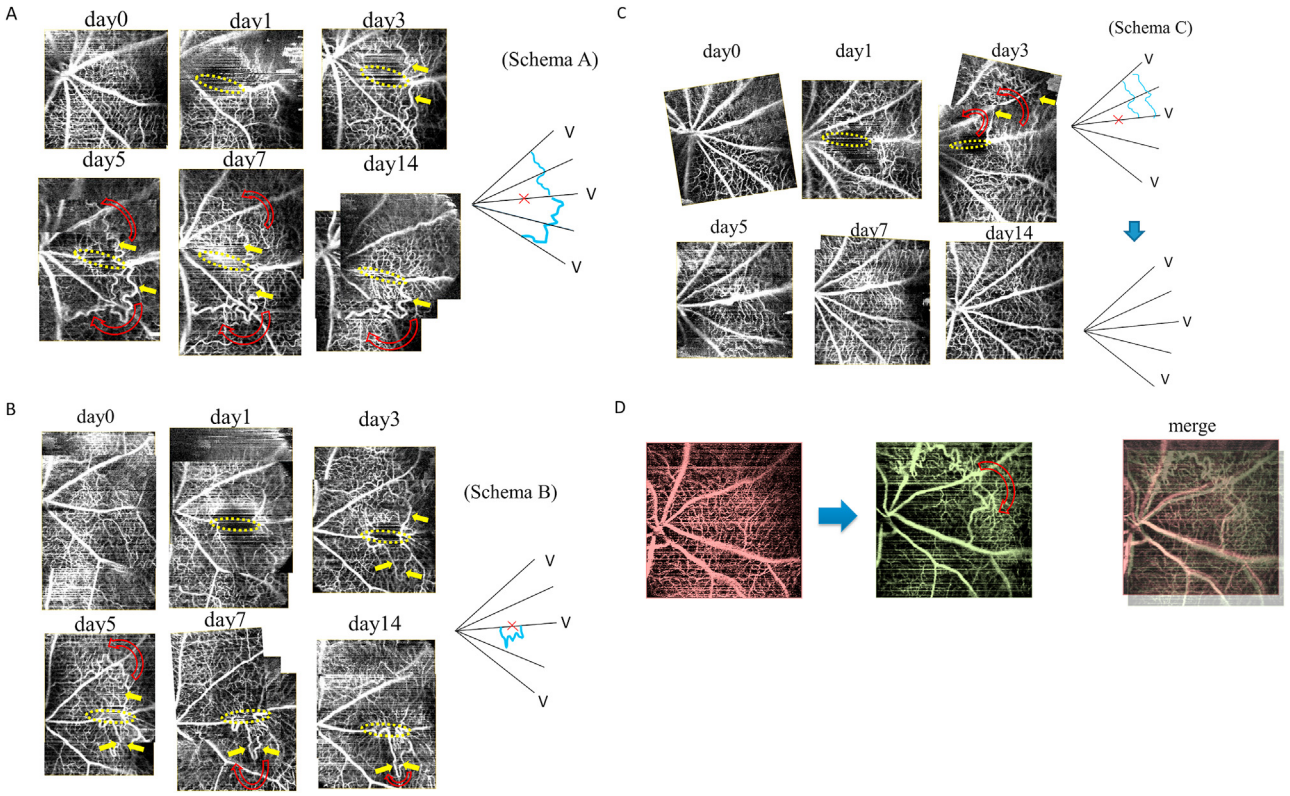

Figure 1. OCTA image for normal course after vein occlusion by PC. (Note that all OCTA images shown above may contain artifact from OCTA itself). A: Collateral blood vessels flow into the nearest adjacent vein from the distal portion of the occluded vein (Type 1). Day 1, the occluded target vein (yellow oval). Day 3, collateral blood vessels (yellow arrows) flowed into other veins from the distal part of occluded vein. Day 5 and 7, collateral blood vessels became much clearer. Day 14, collateral blood vessels in the lower part of this image maintained clear visibility; in contrast, collateral blood vessels in the upper part of the image became obscured. The blood flow directions of the collateral blood vessels are indicated as red hollowed arrows. Right schema A: the red cross shows the point of occlusion. Black radial lines represent the retinal vessels. The blue tortured lines represent newly formed collateral vessels. As illustrated in the right schema A, collateral blood vessels flow into the nearest adjacent vein from the distal portion of the occluded vein. B: Collateral blood vessels flow into the same vein and collateral vessels detour (Type 2). The target occluded vein at day 1 (yellow oval). At day 3, collateral blood vessels (yellow arrows) flowed into other veins from the distal part of the occluded vein; and collateral blood vessels were seen flowing into the same vein in the area proximal to the distal region. By day 5, detouring collateral blood vessels became prominent; in contrast, collateral blood vessels in the upper portion of the image became obscured. The blood flow directions of the collateral blood vessels are indicated as red hollowed arrows. Right schema B: the red cross shows the occlusion point. Radial black lines represent the retinal vessels. The blue tortured line represents the newly formed collateral vessels. As illustrated in the right schema B, some collateral blood vessels flow into the same vein and some collateral vessels detoured. C: Reperfusion of the occluded vein after laser irradiation (Type 3). The target occluded vein at day 1 (yellow oval). At day 3, collateral blood vessels flowed into other veins from the distal part of the occluded vein. At day 5, the laser irradiation occluded vein was reperfused, and no collateral vessels were observed after this point. The blood flow directions of the collateral blood vessels are indicated as red hollowed arrows. Right schema C: the red cross shows the occlusion point. Black radial lines represent the retinal vessels. The blue tortured line represents newly formed collateral vessels. As illustrated in the right schema, the vein that was occluded following laser irradiation became reperfused. D: Comparison of OCTA imaging before and after laser irradiation. Left: prior to PC; center: after collateral vessel formation; right: merged image. The blood flow directions of the collateral blood vessels are indicated as red hollowed arrows. Comparing the morphology of the blood vessels before vascular occlusion and after collateral vessels were established, the originally present micro blood vessels became prominent and subsequently became collateral vessels.

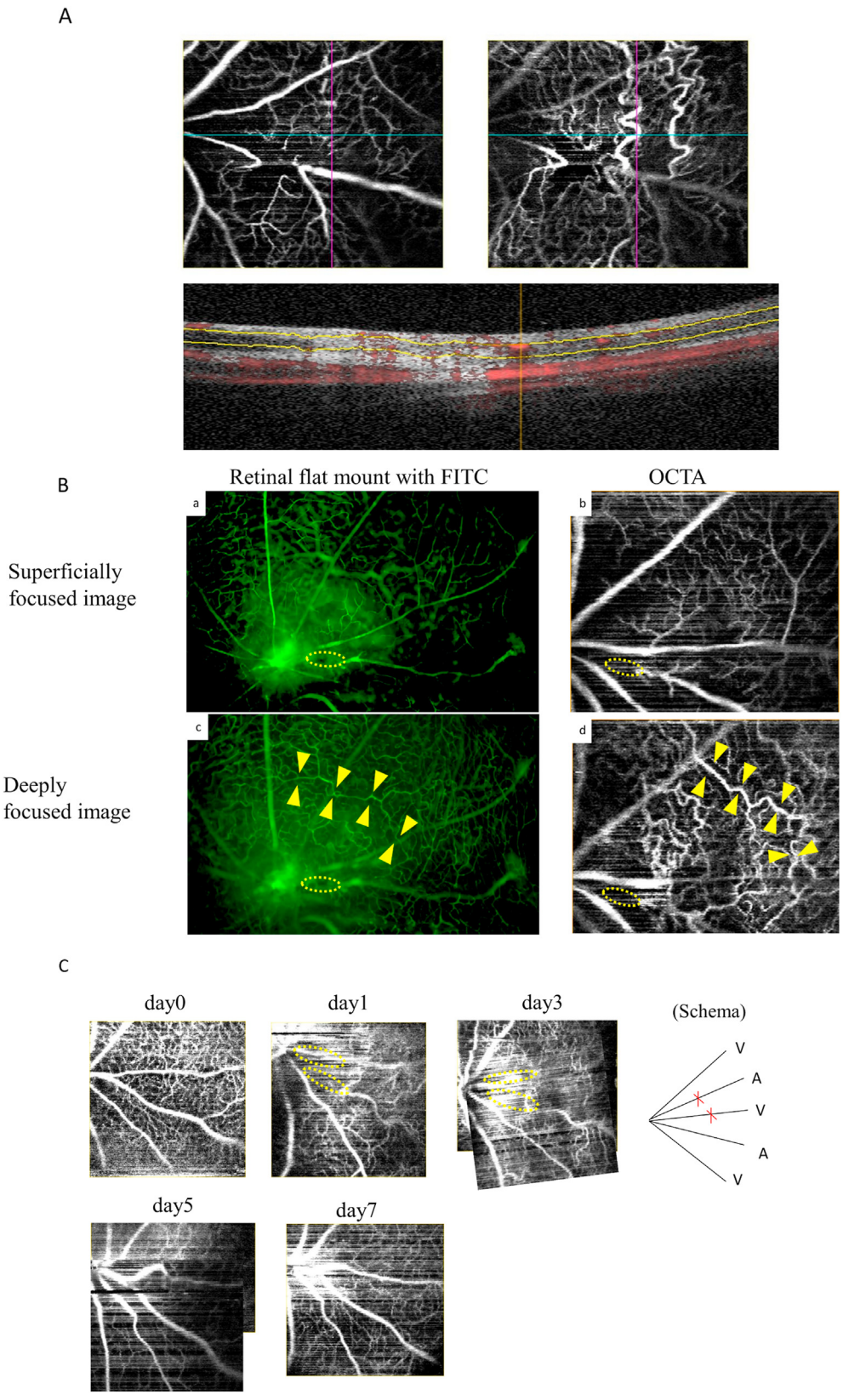

Figure 2. Analysis for localization of collateral vessels by OCTA and relationship between retinal blood flow and collateral vessels formation. (Note that all OCTA images shown above may contain artifact from OCTA itself). A: Visualization of collateral vessels in the deep capillary bed of the retina by OCTA. Upper left: OCTA en-face image of the surface layer of the retina. Upper right: OCTA en-face image of the deep layer of the retina (note that the collateral vessels are only seen clearly in this layer). Lower: OCTA B-scan image of the retina (red dots indicate the presence of blood flow). The upper yellow line indicates the superficial retinal capillary bed. The superficial capillary bed exists above the upper yellow line. The lower yellow line indicates the deep capillary bed of the retina. The deep capillary bed exists between the upper and lower yellow lines. Both the en-face and B-scan images confirmed that the collateral vessels were located in the deep capillary bed of the retina. B: Collateral vessels by the layers of the retina observed in retinal flat mounts and OCTA images. a: Superficially focused image of a retinal flat mount. b: Superficially focused image from OCTA. c: Deeply focused image of a retinal flat mount. d: Deeply focused image from OCTA. Similar to the OCTA image, the collateral vessels were located in the deep capillary bed of the retina as observed in retinal flat mounts labeled by FITC perfusion. Note that the collateral vessels are prominent in the deeply focused image, by contrast they are absent in the superficially focused image (collateral blood vessels are shown along the yellow triangle, the occluded vein is shown in the yellow oval). C: Photocoagulation of one vein and one adjacent artery as observed by OCTA. At day 1, one vein and one artery adjacent to that vein were occluded (yellow oval). No collateral vessel formation was observed. Right schema: the red cross shows the occlusion point. Black radial lines represent the retinal vessels. As illustrated in the right schema, after photocoagulation of one vein and one adjacent artery, no collateral vessels were formed.

3. Results

3.1. OCTA imaging of a mouse model of laser-induced RVO

In the mouse RVO model, we observed changes in retinal blood vessels over time. In 11 out of 15 eyes (73%), the occluded blood vessels remained occluded without reperfusion. Among these 11 eyes without reperfusion, the collateral vessels were observed to be flowing into adjacent veins from the distal part of the occluded vein in 9 eyes (60%, Type 1, Figure 1A), and the collateral vessels flowed into the same vein proximal to the distal area in the other 2 eyes (13%, Type 2, Figure 1B). Reperfusion of the occluded blood vessels occurred in 4 of the 15 eyes such that collateral blood vessels subsequently disappeared and were no longer observed (27%, Type 3, Figure 1C).

All collateral vessels were connected vein to vein. No veno-arterial anastomosis was found.

In addition, morphological comparisons of the blood vessels before vascular occlusion and after collateral vessels were established, clearly showed that the pre-existing micro-blood vessels became prominent and could be observed as collateral vessels (Figure 1D).

3.2. Visualization of collateral vessels in the deep capillary bed of the retina by OCTA and fluorescein-labeling of retinal flat mounts

Next, we investigated where and how collateral vessels form in the retina. The auto-segmentation function of OCTA confirmed that the collateral vessels were located deep in the capillary bed of the retina in all 15 eyes in the en-face images, and B-scans showed that there was blood flow within these collateral vessels (Figure 2A). Thus, in both the en-face and B-scan OCTA images, it was confirmed that the collateral vessels were only located in the deep capillary bed of the retina. In addition, we confirmed histologically that the collateral vessels were located in the deep capillary bed of the retina. Histological assessment of fluorescein dye perfused retinal flat mounts further confirmed that the collateral vessels were only located in the deep capillary bed of the retina (Figure 2B).

3.3. Relationship between collateral vessels and circulating blood volume

Collateral vessels were enhanced when only one vein was occluded. In order to confirm that the same phenomenon would happen if the circulating blood volume was decreased, one vein and one artery adjacent to the vein were occluded and observed by OCTA. Results showed that no collateral vessels were formed when one vein and one adjacent artery were occluded simultaneously, as observed by OCTA (Figure 2C).

3.4. OCTA imaging of S1PR1 agonist and inverse agonist administration in a mouse RVO model

We assessed the appearance of retinal blood vessels between eyes with no PC and no drug administration (sham group), no PC and SEW-administration (sham + SEW group), and no PC and VPC-administration (sham + VPC group). The number of collateral vessels was counted by two masked independent graders. Results showed that no collateral vessels were formed in any of the three groups (Figure 3A, Figure 4A).

The group administered SEW, an agonist of S1PR1 (RVO + SEW group: 9 eyes), and the group administered VPC, an inverse agonist (RVO + VPC group: 7 eyes), were imaged to evaluate the state of the retinal blood vessels including collateral vessels using OCTA (as described above) at time points prior to and at days 1, 3, 5, and 7 post-PC. We compared the findings among the RVO + SEW, RVO + VPC, and normal RVO groups (15 eyes) to determine how the vascular changes occur.

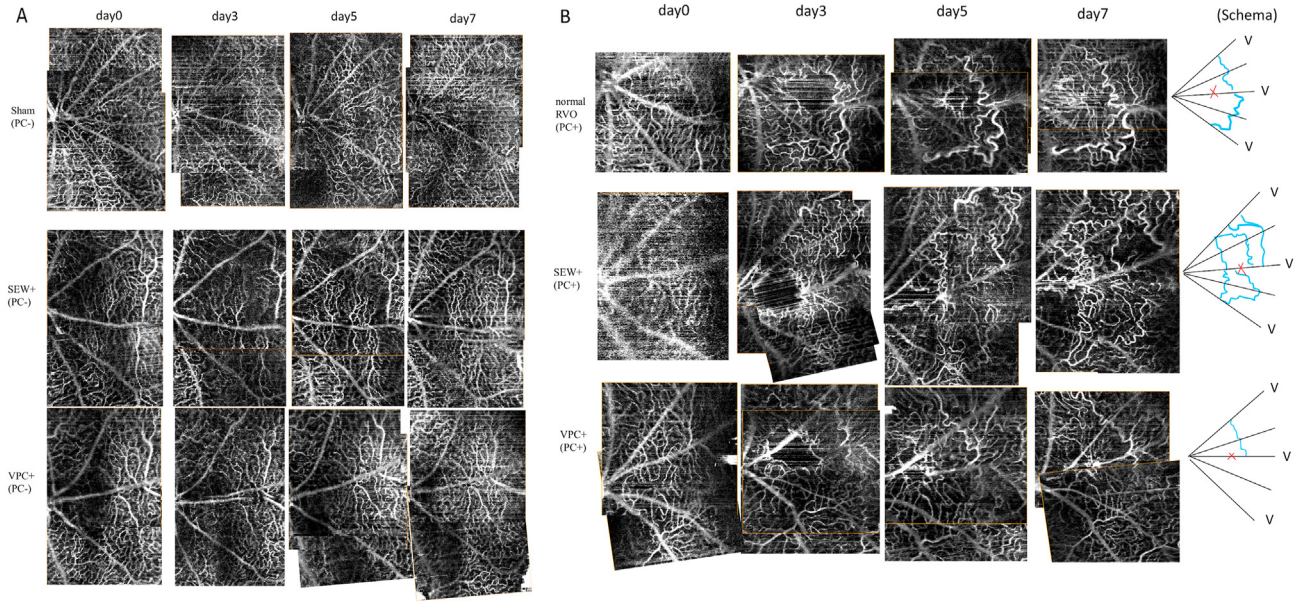

Figure 3. OCTA images under influence of pro-and anti-S1PR1 agent. (Note that all OCTA images shown above may contain artifact from OCTA itself). A: OCTA imaging of S1PR1 agonist and inverse agonist administration in the deep capillary bed of the retina in the no PC model. Upper row: sham model (no PC and no drug administration). Middle row: sham + SEW model (no PC and SEW administration). Lower row: sham + VPC model (no PC and VPC administration). The appearance of the retinal blood vessels did not change, and no collateral vessel formation occurred in the sham model, sham + SEW administration, and sham + VPC administration groups (images show the deep capillary bed of the retina). B: OCTA imaging of S1PR1 agonist and inverse agonist administration in the deep capillary bed of the retina in the RVO model. Upper row: normal RVO model (no drug administration). Middle row: RVO + SEW (SEW-administration). Lower row: RVO + VPC (VPC-administration). The number of collateral vessels in the RVO + SEW group was significantly greater than in the normal RVO group, and RVO + VPC group (both, $p < 0.0001$). The number of collateral vessels in the RVO + VPC group tended to be smaller than in the normal RVO group, although this difference was not statistically significant ($p = 0.1427$). Right schema: the red cross shows the occlusion point. Black radial lines represent the retinal vessels. The blue tortured line represents the newly formed collateral vessels. As illustrated in the right schema, the RVO + SEW group tended to have more collateral vessels than the normal RVO group, and the RVO + VPC group tended to have fewer collateral vessels than the normal RVO group.

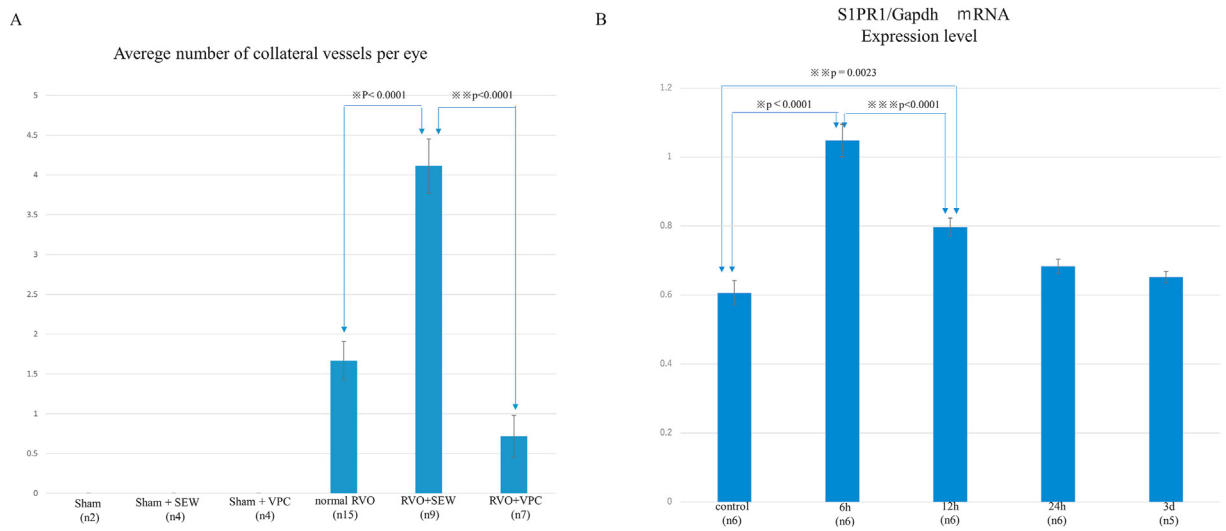

Figure 4. A: Average number of collateral vessels per eye. The average number of collateral vessels per eye was 1.66 in the normal RVO group, 4.11 in the RVO + SEW group, and 0.71 in the RVO + VPC group. The number of collateral vessels differed among the normal RVO group, RVO + SEW group, and RVO + VPC group ($p < 0.0001$). In addition, the number of collateral vessels in the RVO + SEW group was also significantly higher than in the normal RVO group and RVO + VPC group ($p < 0.0001$ for both groups). The number of collateral vessels in the RVO + VPC group tended to be smaller than in the normal RVO group, although the difference was not statistically significant ($p = 0.1427$). B: RT-PCR for S1PR1 expression in the whole retina. Differences in the mean levels of S1PR1 expression were observed between the control group (no laser irradiation and no drug administration), and at time points 6 h, 12 h, 24 h, and 3 days after laser irradiation ($p < 0.0001$). The levels of S1PR1 expression 6 h ($p < 0.0001$) and 12 h ($p = 0.0023$) after laser irradiation were significantly higher than the sham, and these levels then gradually decreased and did not increase thereafter. When comparing S1PR1 expression levels between 6 h and 12 h post-laser irradiation, the expression at 6 h was significantly greater than at 12 h ($p < 0.0001$). The expression of S1PR1 mRNA peaked by about 6 h after blood vessel occlusion, and was significantly greater than control levels.

The number of collateral vessels was counted by two masked independent graders, and these results were analyzed by correlation coefficients and Bland-Altman plots. Analysis showed no apparent differences in evaluation between the two graders (correlation coefficient, RVO + SEW group: $r = 0.91499$, RVO + VPC group: $r = 0.78935$, normal RVO group: $r = 0.72977$. Bland-Altman plot, RVO + SEW group: $p = 0.1690$, RVO + VPC group: $p = 0.1723$, normal RVO group: $p = 0.4985$). The average number of collateral vessels per eye was 1.66 in the normal RVO group, 4.11 in the RVO + SEW group, and 0.71 in the RVO + VPC group (Figure 3B, Figure 4A). The number of collateral vessels statistically differed among the normal RVO group, RVO + SEW group, and RVO + VPC group ($p < 0.0001$). Specifically, the number of collateral vessels in the RVO + SEW group was significantly higher than in the normal RVO group and RVO + VPC group ($p < 0.0001$ for both groups).

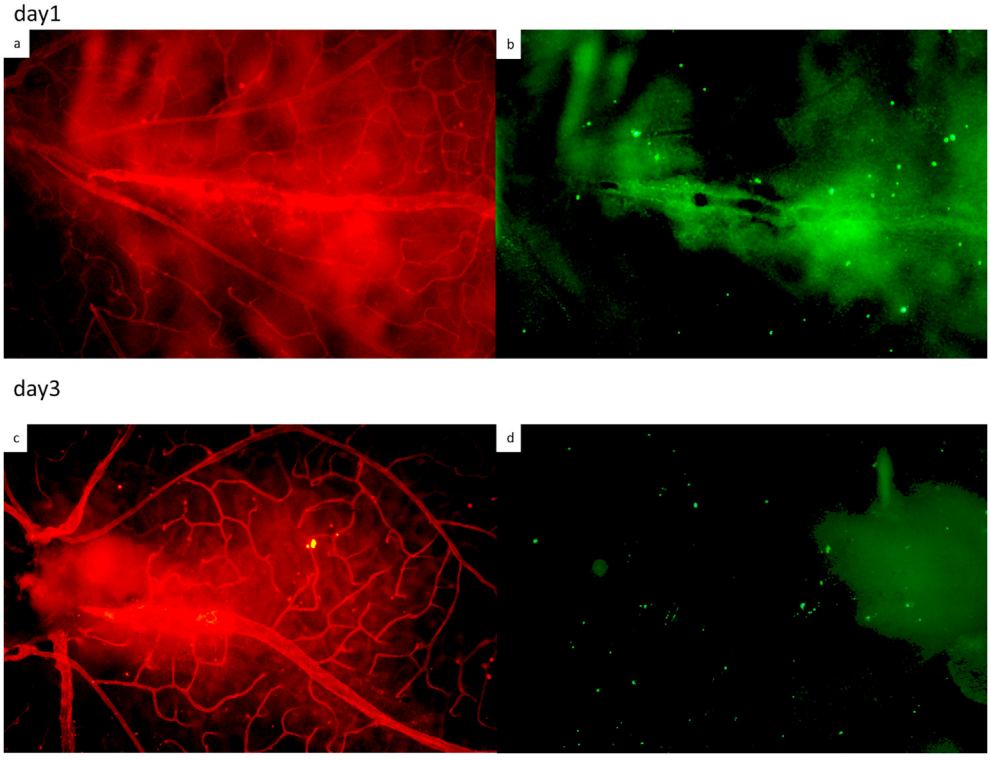

Figure 5. Immunofluorescence imaging of retinal flat mounts. a: Immunohistochemical staining for CD31 at day 1 post-PC. b: Immunohistochemical staining for S1PR1 at day 1 post-PC. c: Immunohistochemical staining for CD31 at day 3 post-PC. d: Immunohistochemical staining for S1PR1 at day 3 post-PC. White oval: occluded vein. On day 1 post-PC, S1PR1 staining occurred along the laser-occluded blood vessel, but was not present along other blood vessels. There was no prominent staining for S1PR1 along the occluded blood vessels after the first day post-PC.

The number of collateral vessels in the RVO + VPC group tended to be smaller than in the normal RVO group, but no statistically significant difference was found ($p = 0.1427$).

3.5. qRT-PCR for S1PR1 in whole retinas

The differences in mean S1PR1 expression levels were assessed between controls (no PC and no drug administration) and at time points 6 h, 12 h, 24 h, and 3 days post-PC ($p < 0.0001$). The S1PR1 expression levels at 6 h ($p < 0.0001$) and 12 h ($p = 0.0023$) post-PC were significantly higher than control levels. After 12 h, mRNA expression levels gradually decreased and did not increase thereafter (Figure 4B). When comparing S1PR1 expression levels between 6 h and 12 h post-PC, the level at 6 h was significantly higher than at 12 h ($p < 0.0001$). The levels of S1PR1 mRNA peaked around 6 h after blood vessel occlusion, and this increase was significantly greater than control levels.

3.6. Immunofluorescence imaging in retinal flat mounts

To visualize how S1PR1 acts in the retina of RVO model mice, immunohistochemical co-staining for CD31 and S1PR1 was performed in retinal flat mounts. On day 1 after PC, S1PR1 staining occurred along the site of the laser-occluded blood vessels, but did not stain any other vessels (Figure 5). There was almost no S1PR1 staining in blood vessels other than the irradiated vessel. However, by day 3 post-PC, there was no obvious staining for S1PR1 remaining along the occluded vessels (Figure 5).

4. Discussion

There have been many reports pertaining to animal models of RVO [3, 4, 5, 18, 19, 20]. In these previous studies, various methods have been utilized to produce the RVO. Among these, Andreas et al. established a technique for performing PC on retinal blood vessels after administration of Rose Bengal dye as a photosensitizer [3]. This strategy greatly facilitated the ease and use of animal models of RVO over previous models. Moreover, the combination of PC with a photosensitizer is less invasive and minimizes laser damage to the tissue adjacent to the target blood vessels [3]. In recent years, some reports have described next-generation techniques for visualizing animal vasculature by OCTA. Nakagawa et al. succeeded in visualizing choroidal neovascularization in mouse eyes by OCTA [21]. However, there had been only one report of using OCTA to visualize vasculature in an RVO animal model. Wada et al. utilized OCTA in a feline RVO model [14]. While they precisely described the vascular changes after PC, the feline model had limitations in the lack of antibodies against various proteins as well as unknown mRNA sequences that would enable further investigation. Thus, we developed an RVO mouse model similar to that used by Andreas et al. Mice are widely used research animals which are easy to handle and experiments generally show good reproducibility. In addition, mice also have the advantage of a tremendous number of antibodies available against various proteins and known mRNA sequences.

In the clinical setting, we sometimes encounter collateral vessels in human patients. Based on these cases, we hypothesized that the formation of collateral vessels may play important roles in resolving pathological ischemia and vascular congestion. In clinical RVO, Suzuki et al. described that eyes with collateral vessels show reduced central retinal thickness (retinal thickness is mainly attributed to venous congestion) compared with eyes without collateral vessels [1]. Our aim in the present study was to clarify the mechanisms of collateral vessel formation in an experimental mouse model of RVO using OCTA combined with molecular and histological assessments.

First, we succeeded in non-invasively visualizing the process of collateral blood vessel formation over time in a mouse RVO model using OCTA. We found that collateral vessels were not created de novo, but were derived from the capillaries which were present prior to occlusion and which subsequently expanded and became more prominent. Wada et al. made similar observations in their experiments on feline RVO [14]. However, due to the characteristics of OCTA, when retinal blood flow is slow, it does not always depict the actual state of retinal blood flow. Moreover, some artifacts may exist on OCTA images which may not accurately reflect the state of the tissue. For example, Nakagawa et al. described the limited potential of OCTA imaging for accurately estimating CNV lesions due to fibrosis artifacts from the OCTA [21]. Thus, we needed to confirm whether the collateral vessels were actually located in the deep capillary bed of the retina using histological assessments. Similar to the OCTA imaging, histological evaluation showed that the collateral vessels were located only in the deep capillary bed of the retina. This is a very important finding since in human eyes it is impossible to determine if collateral vessels exist only in the deep capillary bed of the retina unless the eye is removed from the body. In previous reports of human RVO, various findings have been obtained using OCTA [1, 8, 9, 10, 11, 12, 13]; for example, it was described that the collateral vessels in human RVO also appeared to be located in the deep capillary bed of the retina using OCTA [8]. Thus, our present study succeeded in confirming the similarity between the location of human and mouse collateral vessels in RVO as far as OCTA is concerned. In addition, even in the actual retinal tissue of mouse RVO model, we succeeded in confirming the collateral vessels exist in the deep capillary bed of the retina. This fact is compatible between OCTA and histology.

Next, we investigated the factors associated with collateral vessel formation in this RVO model. When one vein and one adjacent artery were occluded to reduce blood flow to the occluded vein, no collateral vessels were observed by OCTA. In addition, any collateral blood vessels disappeared when the occluded blood vessels were unexpectedly reperfused. Based on these phenomena, we hypothesized that the volume of circulating blood or shear stress (the frictional force exerted on the blood vessel wall by blood flow) might be related to the formation of collateral vessels in RVO. To test this hypothesis, a shear stress-acting protein or its agonist would need to be administered to RVO mice to confirm how retinal blood vessels change in response. Ichijo and Iwasawa et al. described how shear stress applied to occluded blood vessels led to the formation of collateral vessels in their experimental cerebral infarction model [15, 22, 23]. Similarly, Lloyd et al. described how shear stress is involved in the formation of collateral vessels in cardiac ischemia [24]. When shear stress is applied to an occluded blood vessel, the shear stress itself acts as an agonist to stimulate S1PR1 on the vascular endothelial cells, eventually producing nitric oxide (NO) and dilating the capillaries such that they become collateral blood vessels (vasodilation pathway) [15]. It is possible that the same mechanism exists not only in the brain and heart but also in the retina of the eye, whereby collateral vessels occur via S1PR1 due to shear stress when the retinal vein is mechanically occluded. Thus, we selected S1PR1 as a representative shear stress associated protein in the present study. For this experiment, we assessed the effects of applying these agents by comparing the number of collateral vessels formed after laser induced RVO. Results showed that the number of collateral vessels in the agonist-administered group was greater than in the normal RVO group. Conversely, the number of vessels was lower in the inverse agonist-administered group than in the normal RVO group. In addition, when the agonist or the inverse agonist of S1PR1 was administered to mice which did not receive PC, there was no change in the state of the retinal blood vessels. From this we concluded that the S1PR1 agonists and inverse agonists were effective only when shear stress was present. Furthermore, we investigated mRNA expression levels in whole retinas from the laser-induced RVO model by qRT-PCR. Results showed that the amount of S1PR1 mRNA peaked at 6 h after blood vessel occlusion, and this was significantly higher than in control mice. Similarly, in a previous report utilizing a mouse cerebral infarction model, Ichijo described that the S1PR1 mRNA levels peaked 7 days after blood vessel occlusion [22]. We also investigated the immunohistochemical co-staining of CD31 and S1PR1 in retinal flat mounts. We found that on day 1 post-PC, S1PR1 staining occurred along the laser-occluded blood

vessels, however, there was no apparent S1PR1 positive tissue in the samples at any other time point. These results support our hypothesis that the volume of circulating blood or presence of shear stress might be related to the formation of collateral vessels in the RVO model.

We should also note the limitations of our study. First, our model is induced by PC in which the vessels are suddenly and artificially occluded. This is in contrast to clinical RVO vein occlusion which occurs by thrombus under circumstances of systemic hypertension and/or arteriosclerosis. This may represent a substantial difference between our mouse model and the human disease. Moreover, the mice used in this experimental model are young and do not have hypertension or arteriosclerosis. For this reason, it would be desirable to conduct experiments with mice having a background such as hyperglycemia, hyperlipidemia, or hypertension in order to more closely correlate these findings with the human clinical condition. In addition, the observation period of this experimental model was short, and the presence of further long-term vascular changes is unclear. It would be informative to follow up on these RVO model mice for longer durations in order to determine how retinal vasculature and shear stress change over longer periods of time. Lastly, in this study we focused only on S1PR1 as a shear stress factor. Obviously, it is highly possible that unknown factors other than S1PR1 or shear stress act on the formation of collateral vessels. For example, Kedar et al. described that MAGI1 (Membrane Associated Guanylate Kinase, WW And PDZ Domain Containing 1) on vascular endothelial cells is activated by shear stress and produces NO [25]. In addition, Belting and Gemma et al. described that microvascular endothelial cells release microparticles which are rich in tissue factor (TF) that promotes post-ischemic collateral vessel formation, and this pathway has no known relationship to shear stress [26, 27].

This study is of particular significance for several reasons. First, we succeeded in elucidating the process of collateral blood vessel formation in a mouse RVO model using OCTA. Furthermore, in this mouse RVO model, we confirmed that the collateral vessels were located in the deep capillary bed of the retina by both OCTA and histological assessment of retinal tissue, similar to the location of human collateral vessels. This suggests that it may be possible to conduct research in the mouse RVO model that will lead to further elucidation of the pathology of RVO, which is likely to be applicable to humans. In this study, we also uncovered the relationship between shear stress and S1PR1 as a factor in collateral vessel formation in RVO. Further research is needed to fully clarify the process of collateral vessel formation in RVO.

Declarations

Author contribution statement

Hajime Takahashi: Conceived and designed the experiments; Performed the experiments; Analyzed and interpreted the data; Contributed reagents, materials, analysis tools or data; Wrote the paper.

Kazuki Nakagawa, Hidetsugu Mori: Conceived and designed the experiments; Contributed reagents, materials, analysis tools or data.

Haruhiko Yamada: Conceived and designed the experiments; Wrote the paper.

Shimpei Oba, Keiko Toyama: Analyzed and interpreted the data.

Kanji Takahashi: Conceived and designed the experiments; Wrote the paper.

Funding statement

This work was supported by KAKENHI Grant in-Aid for Scientific Research C (issue number: 18K094309) and Osaka Eye Bank Research Grant 2019.

Data availability statement

Data will be made available on request.

Declaration of interests statement

The authors declare no conflict of interest.

Additional information

No additional information is available for this paper.

Acknowledgements

We gratefully acknowledge the work of past and present members of our laboratory and medical office members (special thanks to Motoki Kimura for his Osaka eye bank research).

References

[1] Norihiro Suzuki, Yoshio Hirano, Taneto Tomiyasu, Ryo Kurobe, Yusuke Yasuda, Yuya Esaki, Tsutomu Yasukawa, Munenori Yoshida, Yuichiro Ogura, Collateral vessels on optical coherence tomography angiography in eyes with branch retinal vein occlusion, Br. J. Ophthalmol. 103 (10) (2019 Oct) 1373–1379.

[2] N.L. Christoffersen, M. Larsen, Pathophysiology and hemodynamics of branch retinal vein occlusion, Ophthalmology 106 (11) (1999 Nov) 2054–2062.

[3] Andreas Ebneter, Cavit Agca, Chantal Dysli, S. Martin, Zinkernage, investigation of retinal morphology alterations using spectral domain optical coherence tomography in a mouse model of retinal branch and central retinal vein occlusion, PloS One 10 (3) (2015), e0119046.

[4] Shinichiro Fuma, Anri Nishinaka, Yuki Inoue, Kazuhiro Tsuruma, Masamitsu Shimazawa, Mineo Kondo, Hideaki Hara, A pharmacological approach in newly established retinal vein occlusion model, Sci. Rep. 7 (2017) 43509.

[5] Han Zhang, Koh-Hei Sonoda, Hong Qiao, Toru Oshima, Toshio Hisatomi, Tatsuro Ishibashi, Development of a new mouse model of branch retinal vein occlusion and retinal neovascularization, Jpn. J. Ophthalmol. 51 (2007) 251–257.

[6] Richard F. Spaidea, James G. Fujimoto, Nadia K. Waheed, Srinivas R. Sadda, Giovanni Staurenghi, Optical coherence tomography angiography, Prog. Retin. Eye Res. 64 (May 2018) 1–55.

[7] Talisa E de Carlo, Andre Romano, Nadia K. Waheed, S Duker Jay, A review of optical coherence tomography angiography (OCTA), Int. J. Retina Vitreous 1 (2015) 5.

[8] K. Bailey Freund, David Sarraf, C.S. Belinda, M.D. Leong, Association of optical coherence tomography angiography of collaterals in retinal vein occlusion with major venous outflow through the deep vascular complex, JAMA Ophthalmol. 136 (11) (2018 Nov) 1262–1270.

[9] S. Bonnin, V. Mané, A. Couturier, et al., New insight into the macular deep vascular plexus imaged by optical coherence tomography angiography, Retina 35 (11) (2015) 2347–2352.

[10] Kotaro Tsuboi, Hirofumi Sasajima, Motohiro Kamei, Collateral vessels in branch retinal vein occlusion anatomic and functional analyses by OCT angiography, Ophthalmol. Retina 3 (9) (2019) 767–776.

[11] Hee Eun Lee, Yiyang Wang, Alaa E. Fayed, Amani A. Fawzi, Exploring the relationship between collaterals and vessel density in retinal vein occlusions using optical coherence tomography angiography, PloS One 14 (7) (2019), e0215790.

[12] Taneto Tomiyasu, Yoshio Hirano, Munenori Yoshida, Norihiro Suzuki, Takeshi Nishiyama, Akiyoshi Uemura, Tsutomu Yasukawa, Yuichiro Ogura, Microaneurysms cause refractory macular edema in branch retinal vein occlusion, Sci. Rep. 6 (2016) 29445.

[13] Norihiro Suzuki, Yoshio Hirano, Munenori Yoshida, Taneto Tomiyasu, Akiyoshi Uemura, Tsutomu Yasukawa, Yuichiro Ogura, Microvascular abnormalities on optical coherence tomography angiography in macular edema associated with branch retinal vein occlusion, Am. J. Ophthalmol. 161 (2016 Jan) 12632, e1.

[14] Takanari Wada, Youngseok Song, Tsuneaki Oomae, Kenji Sogawa, Takafumi Yoshioka, Seigo Nakabayashi, Kengo Takahashi, Tomofumi Tani, Akihiro Ishibazawa, Satoshi Ishiko, Akitoshi Yoshida, Longitudinal changes in retinal blood flow in a feline retinal vein occlusion model as measured by Doppler optical coherence tomography and optical coherence tomography angiography, Invest. Ophthalmol. Vis. Sci. 61 (2) (2020 Feb 7) 34.

[15] Eri Iwasawa, Masahiko Ichijo, Satoru Ishibashi, Takanori Yokota, Acute development of collateral circulation and therapeutic prospects in ischemic stroke, Neural Regen. Res. 11 (3) (2016 Mar) 368–371.

[16] Fatemeh Hassani, Bita Ebrahimi, Ashraf Moini, Ghiaseddin Ali, Mahshid Bazrafkan, G. Holamreza Hassanzadeh, Mojtaba Rezazadeh Valojerdi, Chitosan hydrogel supports integrity of ovarian follicles during in vitro culture: a preliminary of A novel biomaterial for three dimensional culture of ovarian follicles, Cell J. 21 (4) (2020 Jan) 479–493.

[17] Carina Scholtysek, Natacha Ipseiz, Christina Böhm, Brenda Krishnacoumar, Stenzel Martin, Tina Czerwinski, Katrin Palumbo-Zerr, Tobias Rothe, Daniela Weidner, Klej Alexandra, Cornelia Stoll, Jörg Distler, Tuckermann Jan, Martin Herrmann, Ben Fabry, Wolfgang H. Goldmann, Georg Schett, Gerhard Krönke, NR4A1 regulates motility of osteoclast precursors and serves as target for the modulation of systemic bone turnover, J. Bone Miner. Res. 33 (11) (2018 Nov) 2035–2047.

[18] Ronald Klein, Barbara Klein, Henkind Paul, Bellhorn Roy, Retinal collateral vessel formation, Investig. Ophthalmol. Vis. Sci. 10 (1971) 471–480.
[19] Wei Chen, Ying Wu, Mi Zheng, Qing Gu, Zhi Zheng, Xin Xia, Establishing an experimental rat model of photodynamically-induced retinal vein occlusion using erythrosin B, Int. J. Ophthalmol. 7 (2) (2014 Apr 18) 232–238.
[20] Meiaad Khayat, Noemi Lois, Michael Williams, Alan W. Stitt, Animal models of retinal vein occlusion, Investig. Ophthalmol. Vis. Sci. 58 (2017) 6175–6192.
[21] Kazuki Nakagawa, Haruhiko Yamada, Hidetsugu Mori, Keiko Toyama, Kanji Takahashi, Comparison between optical coherence tomography angiography and immunolabeling for evaluation of laser induced choroidal neovascularization, PloS One 13 (8) (2018), e0201958.
[22] Masahiko Ichijo, Satoru Ishibashi, Fuying Li, Daishi Yui, Kazunori Miki, Hidehiro Mizusawa, Takanori Yokota, Sphingosine-1-Phosphate receptor-1 selective agonist enhances collateral growth and protects against subsequent stroke, PloS One 10 (9) (2015), e0138029.
[23] Eri Iwasawa, Satoru Ishibashi, Motohiro Suzuki, Fu YingLi, Masahiko Ichijo, Kazunori Miki, Takanori Yokota, Sphingosine-1-Phosphate receptor 1 activation enhances leptomeningeal collateral development and improves outcome after stroke in mice, J. Stroke Cerebrovasc. Dis. 27 (Issue 5) (May 2018) 1237–1251.
[24] W. Lloyd, M.D. Klein, M.D. Enrique Padilla Campos, The embryologic origin of vieussens' ring, JIC 31 (3) (2019). March, 2019 February 24.
[25] Kedar Ghimire, Jelena Zaric, Begoña Alday-Parejo, Jochen Seebach, Mélanie Bousquenaud, Jimmy Stalin, Grégory Bieler, Hans-Joachim Schnittler, Curzio Rüegg, MAGI1 mediates eNOS activation and NO production in endothelial cells in response to fluid shear stress, Cells 8 (5) (2019 May) 388.
[26] M. Belting, M.I. Dorrell, S. Sandgren, E. Aguilar, J. Ahamed, A. Dorfleutner, P. Carmeliet, B.M. Mueller, M. Friedlander, W. Ruf, Regulation of angiogenesis by tissue factor cytoplasmic domain signaling, Nat. Med. 10 (5) (2004 May) 502–509.
[27] Gemma Arderiu Esther Peña, Lina Badimon, Angiogenic microvascular endothelial cells release microparticles rich in tissue factor that promotes postischemic collateral vessel formation, Thromb. Vasc. Biol. 35 (2015) 348–357.